

Supplementary information to:

Implementation and evaluation of the GEOS-Chem chemistry module version 13.1.2 within the Community Earth System Model v2.1

Thibaud M. Fritz¹, Sebastian D. Eastham^{1,2*}, Louisa K. Emmons³, Haipeng Lin⁴, Elizabeth W. Lundgren⁴, Steve Goldhaber³, Steven R. H. Barrett^{1,2}, Daniel J. Jacob⁴

¹Laboratory for Aviation and the Environment, Department of Aeronautics and Astronautics, Massachusetts Institute of Technology, Cambridge, MA 02139, USA

²Joint Program on the Science and Policy of Global Change, Massachusetts Institute of Technology, Cambridge, MA 02139, USA

³Atmospheric Chemistry Observations and Modeling Laboratory, National Center for Atmospheric Research, Boulder, CO, USA

⁴John A. Paulson School of Engineering and Applied Sciences, Harvard University, Cambridge, MA 02138, USA

Correspondence to: Sebastian D. Eastham (seastham@mit.edu)

1. Species mapping between MAM4 and GEOS-Chem species

Table S1 describes the species mapping between MAM4 modal aerosols and GEOS-Chem species.

Table S1: Mapping between MAM4 and GEOS-Chem.

GEOS-Chem species	Mapping to MAM4 species
TSOA0 + ASOAN	soa1_a1 + soa1_a2 + soa2_a1 + soa2_a2
TSOA1 + ASOA1	soa3_a1 + soa3_a2
TSOA2 + ASOA2	soa4_a1 + soa4_a2
TSOA3 + ASOA3	soa5_a1 + soa5_a2
TSOG0	soag0 + soag1
TSOG1 + ASOG1	soag2
TSOG2 + ASOG2	soag3
TSOG3 + ASOG3	soag4

SO4	so4_a1 + so4_a2 + so4_a3 + H2SO4
BCPI	bc_a1
BCPO	bc_a4
OCPI	pom_a1
OCPO	pom_a4
DST1	dst_a1 + dst_a2
DST2	None
DST3	None
DST4	dst_a3
SALA	ncl_a1 + ncl_a2
SALC	ncl_a3

2. Mapping between CLM biogenic emission species and GEOS-Chem species

Table S2 presents the mapping between GEOS-Chem species and MEGAN biogenic emission species as calculated in CLM. Mapping to CAM-chem species is listed in the Supplementary Information of Emmons et al. (2020).

Table S2: Mapping between GEOS-Chem species and MEGAN species in CLM

GEOS-Chem species	MEGAN species in CLM
ISOP	isoprene
MOH	methanol
EOH	ethanol
CH2O	formaldehyde
ALD2	acetaldehyde
ACTA	acetic_acid
ACET	acetone
HCOOH	formic_acid
None	hydrogen_cyanide
CO	carbon_monoxide
C2H6	ethane
C2H4	ethene
C3H8	propane

ALK4	pentane + hexane + heptane + tricyclene
PRPE	propene + butene
TOLU	Toluene
LIMO	Limonene
MTPA	pinene_a + pinene_b + sabinene + carene_3
MTPO	terpinene_g + terpinene_a + terpinolene + myrcene + ocimene_al + ocimene_t_b + ocimene_c_b + thujene_a + 2met_styrene + cymene_p + cymene_o + bornene + fenchene_a + camphene + phellandrene_a + phellandrene_b

3. Emissions mapping in C-GC, C-CC, and S-GC

Table S3 presents the emissions mapping between HEMCO and all three models considered in this study.

Table S3: Emissions mapping from HEMCO to C-GC, C-CC, and S-GC

Emission species	C-GC	C-CC	S-GC
MOH	MOH	CH3OH	MOH
EOH	EOH	C2H5OH	EOH
ROH	ROH	-	ROH
C2H6	C2H6	C2H6	C2H6
C3H8	C3H8	C3H8	C3H8
C4H10	ALK4	BIGALK	ALK4
C5H12	ALK4	BIGALK	ALK4
C6H14	ALK4	BIGALK	ALK4
C2H4	C2H4	C2H4	C2H4
PRPE	PRPE	C3H6	PRPE
C2H2	C2H2	C2H2	C2H2
BENZ	BENZ	BENZENE	BENZ
TOLU	TOLU	TOLUENE	TOLU
XYLE	XYLE	XYLENES	XYLE
TMB	-	XYLENES	-
OTAR	-	XYLENES	-
CH2O	CH2O	CH2O	CH2O

ALD2	ALD2	CH3CHO	ALD2
MEK	MEK	MEK	MEK
ACE	-	CH3COCH3	-
HCOOH	HCOOH	HCOOH	HCOOH
C2OH	-	CH3COOH	-
EOH	EOH	C2H5OH	EOH
MACR	MACR	MACR	MACR
ACET	ACET	CH3COCH3	ACET
BCPI	bc_a*	bc_a*	BCPI
OCPI	pom_a*	pom_a*	OCPI
SO4	so4_a1/so4_a2	so4_a1/so4_a2	SO4

4. Dust emissions in CESM

Emissions of dust in CESM are calculated through the Community Land Model (CLM), with a resolution-dependent scaling factor applied. For this work, we use the same scaling factor (0.24) for both C-CC and C-GC, resulting in dust emissions of 5,894 Tg per year. This is significantly greater than the ~3,000 Tg/yr reported by Emmons et al. (2020), due to the use of a different scaling factor and resolution in that work.

As discussed by Tilmes et al. (2016), the dust emissions scaling factor in CESM is typically tuned to achieve an annual mean dust aerosol optical depth (AOD) of 0.025 – 0.030. We find AODs of 0.04 in C-GC, and 0.08 in C-CC. This suggests that dust removal in C-GC is roughly twice as efficient as in C-CC. This implies that the scaling factor should be reduced in future usage of C-GC or C-CC. The combination of C-GC’s relatively small overestimate in dust AOD and the large total dust emissions also implies that dust scavenging in C-GC may be too rapid.

5. Representations of in-cloud sulfur oxidation in the GEOS-Chem chemistry modules and MAM

Two representations of in-cloud sulfur oxidation exist in C-GC: from the GEOS-Chem chemistry modules and in MAM. For C-GC, we choose to use the GEOS-Chem representation of in-cloud sulfur oxidation, such that the GEOS-Chem chemistry module remains identical to that of the GEOS-Chem CTM. However, this makes C-GC and C-CC, both embedded in CESM2, rely on different processes to perform sulfur oxidation in clouds. The routines responsible for in-cloud sulfur oxidation in MAM are bypassed when running C-GC.

Previous versions of C-GC double counted in-cloud sulfur oxidation. We here perform two test runs of C-GC for January 2015 before and after the sulfur oxidation bugfix - which introduces the bypass of the routines in MAM responsible for in-cloud sulfur oxidation. Figures S1 and S2 display the relative difference in zonal SO_2 and SO_4 attributable to the MAM in-cloud sulfur oxidation. Implementing this bugfix increases SO_2 and decreases SO_4 , enhancing the SO_2 burden by ~5 to 10%.

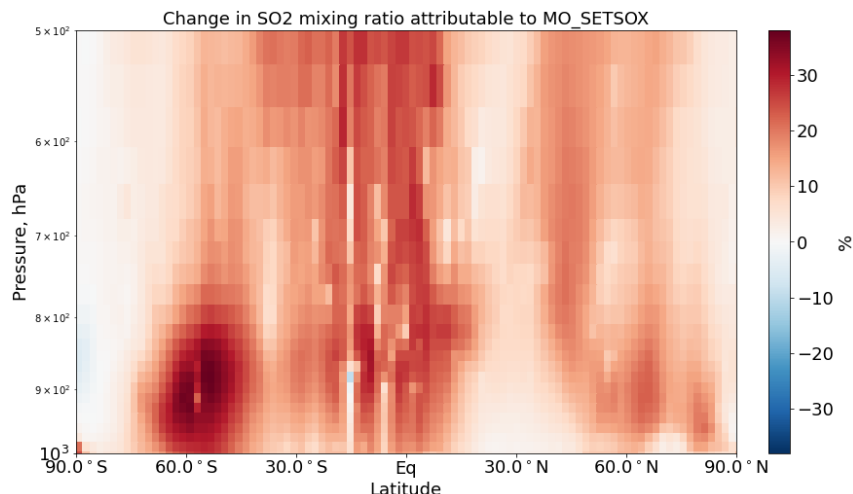


Figure S1: Relative difference in zonally-averaged sulfur dioxide mixing ratios up to 500 hPa due to in-could sulfur oxidation as evaluated by MAM.

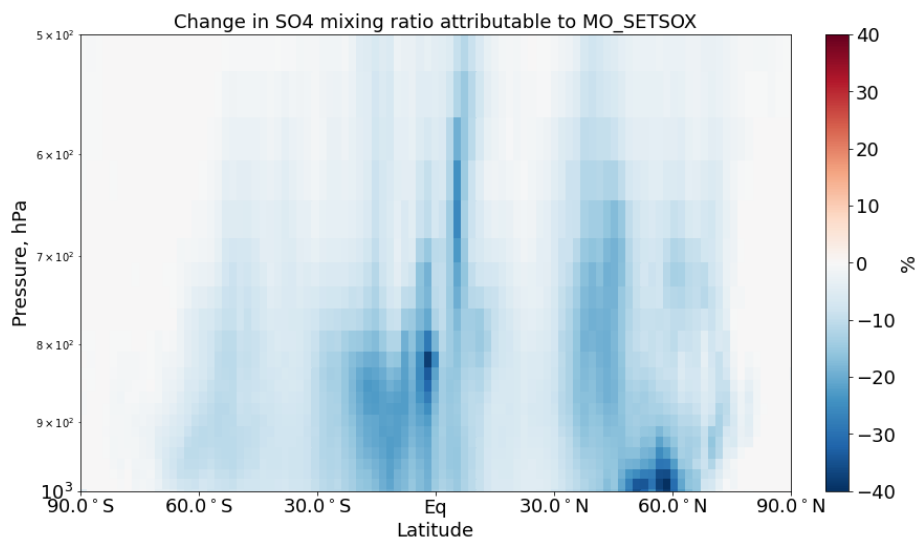


Figure S2: Relative difference in zonally-averaged sulfate aerosols mixing ratios up to 500 hPa due to in-could sulfur oxidation as evaluated by MAM.

6. Non-linear chemistry during the Antarctic spring

This section focuses on the changes in atmospheric composition above the South Pole for C-GC and S-GC. Figures S3, S4, and S5 respectively display active chlorine, inactive chlorine, and ozone, averaged over the 80°S - 90°S latitude band for C-GC and S-GC for 2015 and 2016.

For both C-GC and S-GC, we observe strong production of active chlorine during austral winter. The peak active chlorine mixing ratio is greater in S-GC by ~15%. Correspondingly, we find that reservoir species of chlorine are depleted during austral winter in the 10 to 100 hPa altitude band in both models.

In both models, we find that ozone is depleted during the Antarctic spring (from September to December) due to the presence of active halogens and sunlight. We find that the magnitude of the ozone hole matches from one year to the other in both models (2015 appears to have a more significant ozone hole than 2016). We also find that during the Antarctic spring, ozone around 10 hPa increases in both C-GC and S-GC.

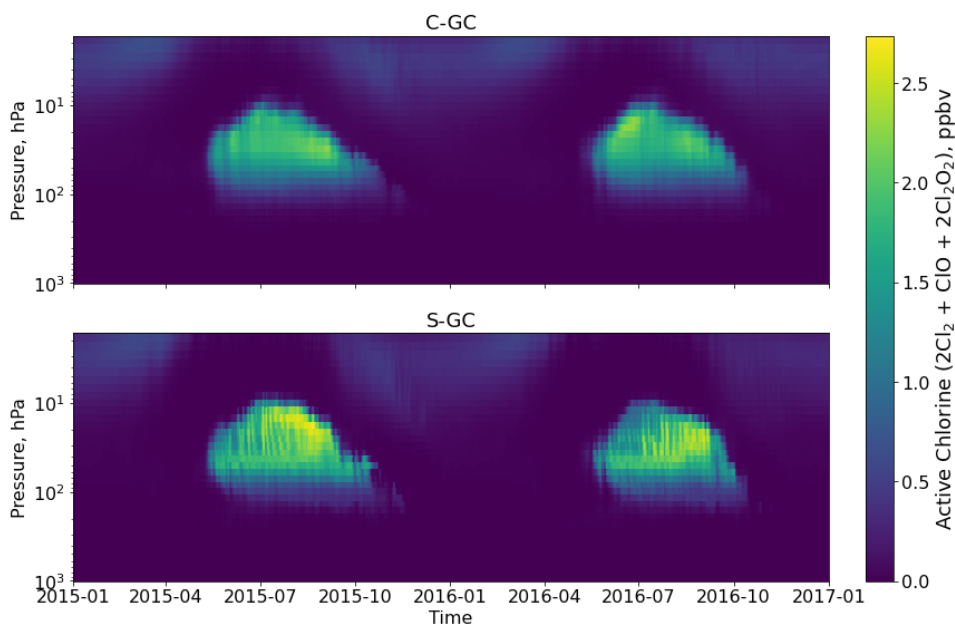


Figure S3: Temporal evolution of active chlorine averaged over the 80°S - 90°S latitude band for C-GC (top) and S-GC (bottom).

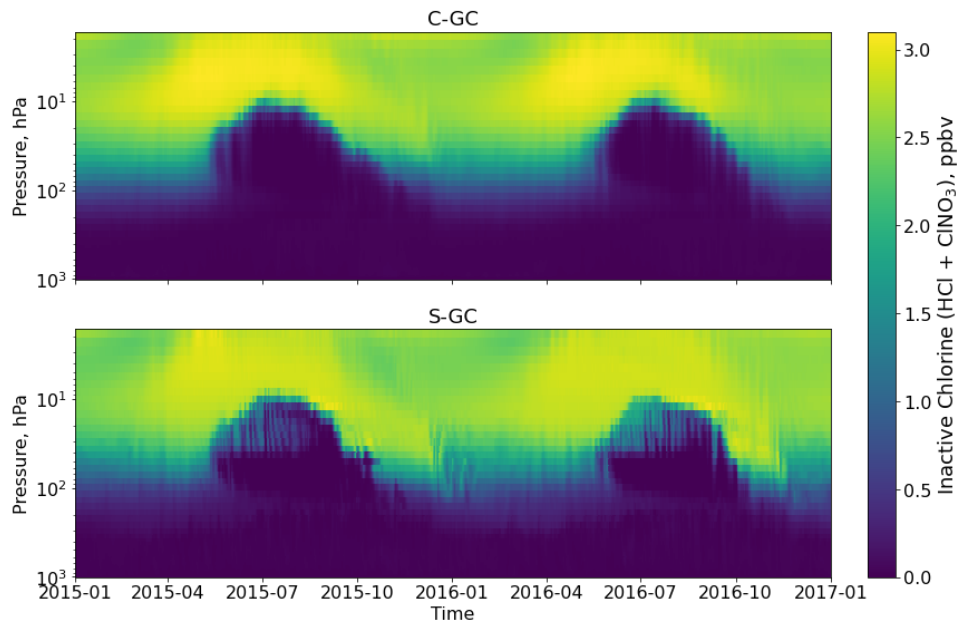


Figure S4: Temporal evolution of inactive chlorine averaged over the 80°S - 90°S latitude band for C-GC (top) and S-GC (bottom).

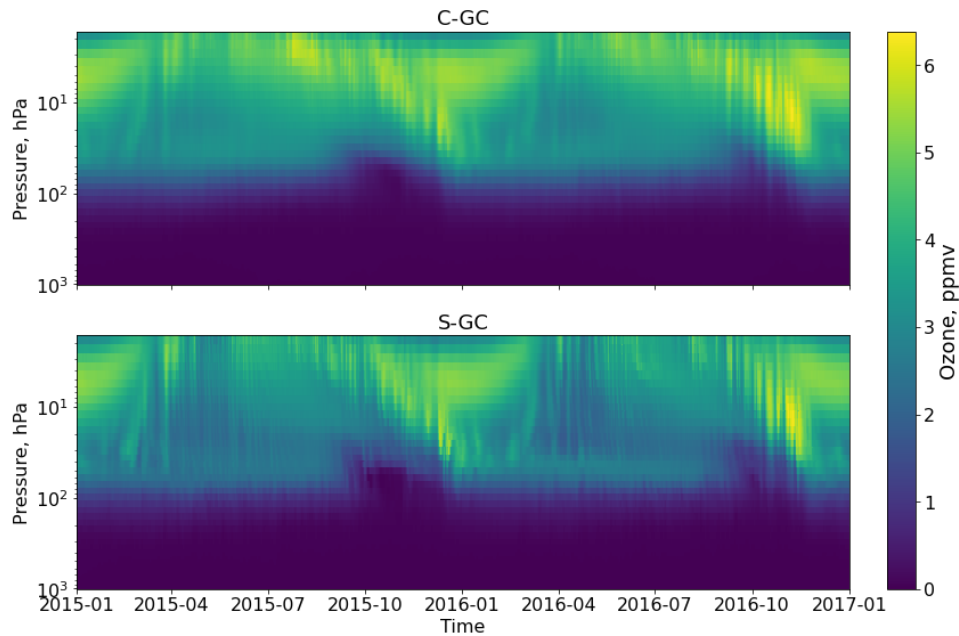


Figure S5. Temporal evolution of ozone averaged over the 80°S - 90°S latitude band for C-GC (top) and S-GC (bottom).

Figure S6 displays the minimum ozone column in the 80°S - 90°S latitude band from C-GC and S-GC against measurements from the NASA Ozone Watch (<https://ozonewatch.gsfc.nasa.gov/>, last accessed 7 January 2022).

During the Antarctic spring, we find that C-GC more accurately reproduces the dip in the ozone column, but this could be due to differences in the horizontal resolution. We also find that both models fail to capture the increase in the South Pole ozone column between May and July for both 2015 and 2016.

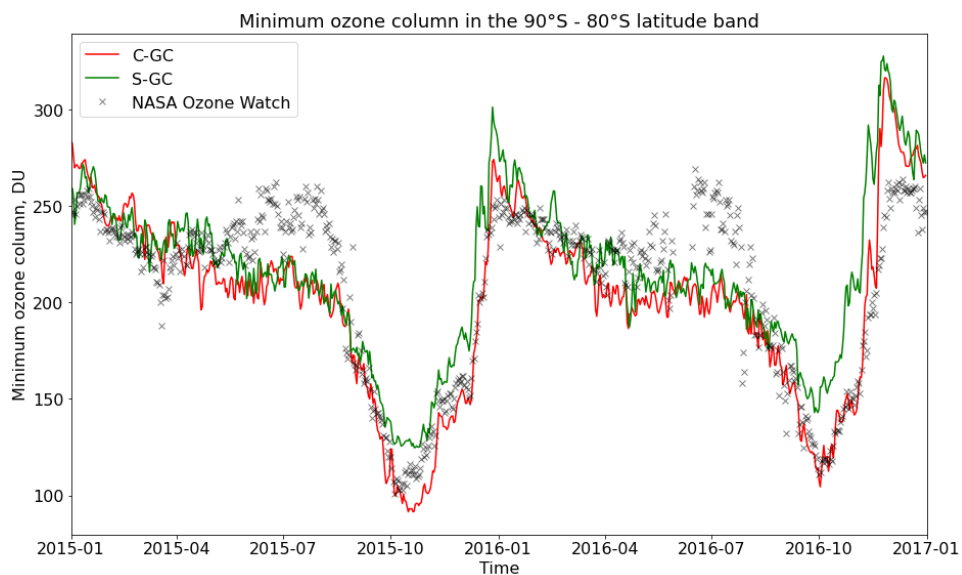


Figure S6: Temporal evolution of minimum ozone column averaged over the 80°S - 90°S latitude band for C-GC (blue) and the GEOS-Chem CTM (red).